



HAL
open science

Ortho–para-H₂ conversion processes in astrophysical media

François Lique, Pascal Honvault, Alexandre Faure

► **To cite this version:**

François Lique, Pascal Honvault, Alexandre Faure. Ortho–para-H₂ conversion processes in astrophysical media. *International Reviews in Physical Chemistry*, 2014, 33 (1), pp.125-149. 10.1080/0144235X.2014.897443 . hal-04159232

HAL Id: hal-04159232

<https://hal.science/hal-04159232>

Submitted on 18 Feb 2024

HAL is a multi-disciplinary open access archive for the deposit and dissemination of scientific research documents, whether they are published or not. The documents may come from teaching and research institutions in France or abroad, or from public or private research centers.

L'archive ouverte pluridisciplinaire **HAL**, est destinée au dépôt et à la diffusion de documents scientifiques de niveau recherche, publiés ou non, émanant des établissements d'enseignement et de recherche français ou étrangers, des laboratoires publics ou privés.

Ortho–para- H_2 conversion processes in astrophysical media

François Lique*

*LOMC - UMR 6294, CNRS-Université du Havre,
25 rue Philippe Lebon, BP 540, 76058, Le Havre, France*

Pascal Honvault

*Laboratoire ICB, UMR 6303, CNRS-Université de Bourgogne,
21078 Dijon cedex, France and UFR Sciences et Techniques,
Université de Franche-Comté, 25030 Besançon Cedex, France*

Alexandre Faure

*UJF-Grenoble 1/CNRS, Institut de Planétologie et d'Astrophysique
de Grenoble (IPAG) UMR 5274, Grenoble F-38041, France*

(Dated: March 23, 2022)

Abstract

We report in this review recent fully-quantum time-independent calculations of cross sections and rate constants for the gas phase ortho-to-para conversion of H_2 by H and H^+ . Such processes are of crucial interest and importance in various astrophysical environments. The investigated temperature ranges was 10–1500 K for $\text{H}+\text{H}_2$ and 10–100 K for H^++H_2 . Calculations were based on highly accurate H_3 and H_3^+ global potential energy surfaces. Comparisons with previous calculations and with available measurements are presented and discussed. It is shown that the existence of a long-lived intermediate complex H_3^+ in the (barrierless) H^++H_2 reaction give rise to a pronounced resonance structure and a statistical behaviour, in contrast to $\text{H}+\text{H}_2$ which proceeds through a barrier of ~ 5000 K. In the cold interstellar medium ($T \leq 100$ K), the ortho-to-para conversion is thus driven by proton exchange while above ~ 300 K, the contribution of hydrogen atoms become significant or even dominant. Astrophysical applications are briefly discussed by comparing, in particular, the relative role of the conversion processes in the gas phase (*via* H , H^+ , H_2 and H_3^+) and on the surface of dust particles. Perspectives concerning future calculations at higher temperatures are outlined.

*Electronic address: francois.lique@univ-lehavre.fr

Contents

I. Introduction	4
II. Theoretical methods	6
A. Potential energy surfaces	6
B. Scattering Calculations	10
III. Ortho–para-H₂ conversion processes	14
A. Ortho–para-H ₂ conversion by hydrogen exchange	14
B. Ortho–para-H ₂ conversion by proton exchange	22
IV. Discussion and astrophysical applications	27
V. Conclusion	29
Acknowledgments	29
References	29

I. INTRODUCTION

Hydrogen is the most abundant element in the Universe and molecular hydrogen, H_2 , is the dominant molecule in all astrophysical environments, from the atmospheres of giant (exo)planets to external galaxies. Molecular hydrogen is also used in many industrial applications, and is often discussed as a potential energy carrier for the future. In particular, low-temperature hydrogen plasmas are relevant for many technological plasma applications including fusion. In the interstellar medium (ISM), where stars and planets form, H_2 is produced efficiently *via* the recombination of hydrogen atoms on the surface of sub-micron size dust grains [1]. In the early Universe, where dust grains were absent, the dominant source of H_2 was the associative detachment between H and H^- and, at high density, the three body recombination $\text{H}+\text{H}+\text{H}$ [2]. Molecular hydrogen is a major contributor to the physics and chemistry of astrophysical media and, in particular, it played a fundamental role in the cooling of the gas clouds that gave birth to the very first stars.

Owing to its identical hydrogen nuclei (with nuclear spin $1/2$), H_2 exists in ortho (o- H_2) and para (p- H_2) forms, also called nuclear-spin isomers. In the electronic ground state, the rotational levels of o- H_2 have odd values of the angular momentum j while the levels of p- H_2 have even j values. The internal energy of the newly formed H_2 molecules is expected to depend on the specific formation mechanism but it is generally assumed that H_2 is initially highly excited. The ortho-to-para ratio (OPR) of nascent H_2 is therefore usually taken as its limiting (high temperature) statistical value of 3, which is the ratio of the degeneracies of the ortho ($I=1$) and para ($I=0$) nuclear spin states. The OPR of H_2 formed on cold (<50 K) solid surfaces was studied in several recent experiments and the measured values were indeed found to be consistent with the high temperature limit of 3 (see [3] and references therein). In other processes, the conservation of the total nuclear spin plays a crucial role and, for instance, in the dissociative recombination of H_3^+ with electrons, the OPR of the product H_2 molecules depends on the OPR of the reactant H_3^+ molecules (see [4] and references therein).

In an isolated state, the (radiative) interconversion between the ortho and para states of H_2 is extremely slow, the theoretical time scale being $\sim 5 \times 10^{20}$ s [5], i.e. greater than the age of the Universe. Ortho-to-para conversion (OPC) (also referred as nuclear spin conversion) is also forbidden in non-reactive inelastic collisions. As a result, the OPC can only occur in the gas phase *via* “spin exchange” (reactive) collisions and in the solid phase *via*

interaction with surfaces of magnetic or diamagnetic materials, including amorphous water ice [6]. In both laboratory and space environments, the OPR of H_2 is however not necessarily at thermal equilibrium because the timescale of the OPC process can be significantly longer than the timescale of the thermal evolution (and also than the thermalization time within each modification). Thus, the H_2 OPR measurements reported in the astronomical literature often show values out of equilibrium with the environment temperature, e.g. in planetary atmospheres [7] or in protostellar shocks [8, 9] where the values typically vary from 1 to 3. The OPR value therefore provides a valuable probe of the thermal history and lifetime of the observed astronomical object. In cold interstellar clouds, where H_2 is invisible, the OPR is expected to decrease slowly with temperature (from its initial value of 3) but to remain higher than the thermal equilibrium value ($\sim 4 \times 10^{-7}$ at 10 K) [10]. Indirect evidences based on the observation of deuterated molecules (see [10, 11] and references therein) and ammonia [12, 13] indeed suggest OPR values of $\sim 10^{-3}$. This has important consequences because the OPR of H_2 not only affects the interstellar chemistry but also the molecular excitation (see e.g. [14]) and therefore the cooling by molecular line emission.

In astronomical environments, the OPC rate on solid surfaces is highly uncertain because it strongly depends on poorly known parameters such as the electronic structure of the surface, the residence time of H_2 , the conversion efficiency, etc. [15]. In the gas phase, the conversion can occur through spin-scrambling reactions between H_2 and the most abundant hydrogenated species H , H^+ , H_2 and H_3^+ . The relative contribution of each colliding partner depends on its relative density and on the kinetic temperature. Indeed, because the reactions of H_2 with H and H_2 have substantial barriers (~ 5000 K and $\sim 60\,000$ K, respectively), the OPC in the cold ISM (i.e. $j = 1 \rightarrow 0$) is driven by proton exchange with H^+ and H_3^+ . In warmer regions ($\gtrsim 300$ K), however, reactive collisions with H become efficient. Examples are shock-heated gas, photon dominated regions (PDRs), supernova remnants, and the primordial gas. Finally, in planetary atmospheres where the H_2 density is much larger than in the ISM ($\gtrsim 10^{20}$ cm^{-3}), H_2+H_2 collisions can play an important role despite very low rate coefficients [7].

In the present work, we review recent theoretical work on the OPC of H_2 by hydrogen and proton exchange in the gas phase. These two reactions, $\text{H}+\text{H}_2$ and H^++H_2 (and their isotopic analogs), have become prototypes for triatomic reactions and because of their experimental and theoretical accessibility, they have been studied in much detail, allowing a very

accurate understanding of the dynamics. Surprisingly, however, the specific OPC process has not been the object of many theoretical investigations in the past. Very recently, it has been revisited using full dimensional quantum time-independent approaches combined with high accuracy *ab initio* potential energy surfaces (PES) for H_3 [16] and H_3^+ [17–19]. These triatomic systems are indeed amenable to state-of-the-art computational methods and various measurements have confirmed that theory and experiment have now converged for such elementary reactions, as discussed below. In contrast, only approximate theoretical methods have been applied so far to the four- and five-atom systems H_2+H_2 and H_3^++H_2 . For these important processes, we refer the reader to other recent sources. Thus, for the OPC of H_2 by H_2 , theoretical and experimental results are discussed in [7, 20]. For the OPC of H_2 by H_3^+ , the interested reader can find detailed information on the various recent experimental and theoretical works in [21, 22] and references therein. Finally, for the conversion on solid surface, we refer the reader to the very recent review by Fukutani & Sugimoto [3].

This review is organized as follows: Section II provides a description of the theoretical methods that can be employed for triatomic reactive systems. In Sec. III results are presented for the OPC of H_2 by hydrogen and proton exchange. In Sec. IV, astrophysical applications are discussed. Concluding remarks are drawn in Sec. V.

II. THEORETICAL METHODS

The computation of reactive rate constants usually takes place within the Born-Oppenheimer approximation for the separation of electronic and nuclear motions. Reactive cross sections are thus obtained by solving the motion of the nuclei on an electronic PES, which is independent of the masses and spins of the nuclei.

A. Potential energy surfaces

The PES must be accurate since the dynamical calculations are very sensitive to the PES quality. The most accurate treatments to compute PES are those based on modern methods of *ab initio* quantum chemistry [23]. The process of reactive collision between a diatomic molecule and an atom requires generally, for the PES calculation, the use of *ab initio* methods based on configuration interaction (CI). CI methods like multireference

internally contracted configuration-interaction (MRCI) method [24, 25], which is currently the most accurate method, is generally used to describe all geometries that could be explored by the nuclei during the collisional process.

For light triatomic reactive systems like the $\text{H}+\text{H}_2$ and H^++H_2 systems, Full Configuration Interaction (FCI) method [26, 27] which provides numerically exact solutions (within the atomic basis set) can also be used. This approach is very CPU consuming but can provide a very accurate description of the correlation energy as long as large atomic basis set are used.

For heavier systems or with many degrees of freedom, Multiconfigurational second-order perturbation theory (CASPT2) methods [28, 29] can alternatively be used in order to keep reasonable CPU time without altering too much the accuracy of the PES.

Finally, for reactive systems whose wave function can be reasonably well described by a single determinant wave function, coupled-cluster theory [30] can also provide an accurate estimate of the PES. However, reactive systems are rarely monoconfigurational systems and such approach cannot generally be used.

In the methods described above, the quality of the result is also determined by the choice of atomic orbitals to describe the molecular orbitals and the electronic configuration. The chosen atomic orbitals basis set, from which are built the molecular orbitals, must be large enough to correctly represent the correlation energy and not too extended so that the computation time remains acceptable. The augmented correlation-consistent valence quadruple zeta (aug-cc-pVQZ) or quintuple zeta (aug-cc-pV5Z) basis sets of Dunning and co-workers [31–33] are usually well adapted to interaction PES calculations. In order to get accurate results with respect to the atomic basis set, the energies obtained with the incomplete basis set can be extrapolated to the Complete Basis Set (CBS) limit, employing for example the mixed exponential and Gaussian formula [34, 35]: $E_X = E_{CBS} + Ae^{-(X-1)} + Be^{-(X-1)^2}$, where X denotes the size of the smaller basis and E_{CBS} , A and B are adjustable fitting parameters.

The standard quantum chemistry methods described above are implemented in several widely used numerical codes (MOLPRO [36], GAUSSIAN [37] or MOLCAS [38])

Then, an additional important step related to the interaction PES determination is the building of its analytic representation in order to adequately perform the dynamical calculations. Great care should be taken in order to maintain the accuracy of the *ab initio* PES

in its analytical representation through elaborate fitting techniques. Fitting methods such as the Reproducing Kernel Hilbert Space (RKHS) method [39] or the double many-body expansion (DMBE) [40] theory are generally used to obtain the analytic representations.

Generally, the long range values derived from the *ab initio* calculations are not very accurate as they result from the (small) difference of two large numbers. One should keep in mind the importance of carefully extending the analytical PES values to the long range part which can be more precisely derived from perturbation calculations as a $1/R$ expansion, where R represents the distance between the centers of charge of the two interacting systems. The long range part is then described by the electrostatic, induction and dispersion terms contributing to the total interaction energy of the complex with the proper angular and radial dependences [41]. Small unphysical irregularities of magnitude $\simeq 1 \text{ cm}^{-1}$ at long range can significantly affect the dynamical calculations. These effects are even more crucial in the field of cold and ultra-cold collisions.

The H_3 system considered in the present review can be viewed as a prototype of small polyatomic systems. The corresponding PES has been extensively studied. The first fully *ab initio* PES was published in 1978. Truhlar & Horowitz [42] made an accurate least-squares fit to Liu and Siegbahns calculations [43] of the PES for the $\text{H}+\text{H}_2$ reaction. Approximately a decade later, two refined versions of the H_3 PES, called DMBE [44] and BKMP [45] have been published. Finally, the most recent calculations by Boothroyd et al. [46] and Mielke et al. [47] have been widely used both for $\text{H}+\text{H}_2$ inelastic and reactive collisions, including the isotopic variants. These two PESs generally lead to very good agreement with available experimental data. The *ab initio* H_3 PES of Mielke et al. [47] that will be used for the results reviewed in this work was calculated at the Full Configuration Interaction (FCI) level using a complete basis set extrapolation. It is probably one of the most accurate PES available for a chemical reactions. On this PES, the reaction proceeds through a large barrier of $\simeq 0.4 \text{ eV}$. The van der Waals well associated to the $\text{H}-\text{H}_2$ complex in the entrance channel is about 20 cm^{-1}

About the H_3^+ system also considered in the present review, several global PES covering the whole configuration space are nowadays available in the literature. The first global *ab initio* PES of the ground electronic state of H_3^+ has been published in 2000 and it was based on full configuration interaction (FCI) calculations with a high level basis set [48]. Global PESs of the three lowest electronic singlet states of H_3^+ have been built from the

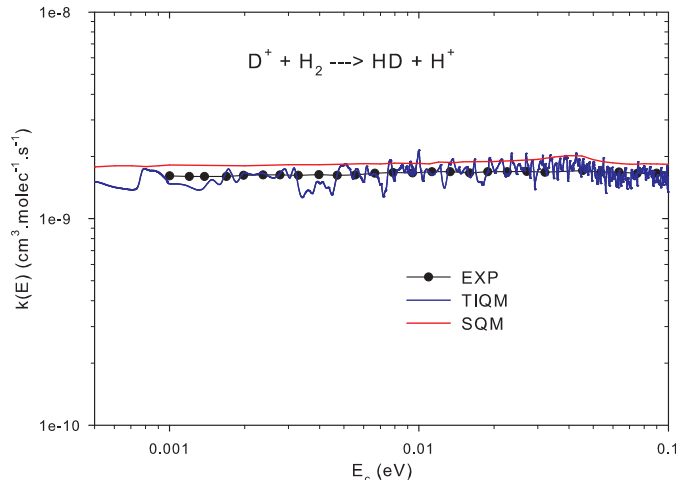


FIG. 1: Rate coefficients for the $D^+ + H_2(v = 0, j = 0) \rightarrow HD + H^+$ reaction. TIQM results (blue line) are compared with the Statistical Quantum Mechanical (SQM) prediction (red line) and the measurements. See the following reference for more details. Reprinted with permission from Ref. [54]. Copyright 2013 American Chemical Society.

diatomics-in-molecule approach [49, 50] or using the DMBE method [51].

Recently, an updated version [52] of the *ab initio* PES of Aguado et al. [48] has been published. In the following section, the results on $H^+ + H_2$ have been obtained on this PES. We therefore recall the main features of this high quality *ab initio* PES. Compared to the previous version published in 2000, new refinements have been indeed added in the present PES, such as more *ab initio* points and the inclusion of a functional form of the long-range electrostatic interaction in the analytical representation. This last point is crucial to compute accurate scattering attributes at low temperature. In addition, the PES is invariant under all permutations of the nuclei and presents a deep well (4.6 eV relative to the $H^+ + H_2$ asymptote) and no barrier in the entrance channel. All approaches are therefore possible and both abstraction and insertion mechanisms can occur. In 2013, quantum mechanical and approximate dynamical calculations have been performed on this PES for the study of the $D^+ + H_2$ reaction [53, 54]. The comparison between the quantum-mechanical rate constant and the measurements showed an excellent agreement as illustrated in Fig. 1. The very good accord between experiment and theory therefore validates the fact that this PES is sufficiently accurate to correctly describe the dynamics of such a reaction.

B. Scattering Calculations

Once the PES has been determined, the reactive cross sections and rate constants are derived from the solution of the nuclear Schrödinger equation within a given PES. Several approaches can be used to determine the reactive cross sections and rate constants. The most widely used approach for reaction dealing with the H_3 and H_3^+ systems are quantum time dependent and time independent methods. Indeed, the large ro-vibrational energy level spacings of H_2 make this system well suited for quantum scattering calculations.

Nevertheless, it is well known that the wave packet method may not be very accurate at low collision energies that characterize the ISM because of difficulties in damping outgoing waves with long de Broglie wavelengths. A quantum time independent treatment seems to be the most reasonable and accurate choice for such studies.

The computation of reactive cross sections is generally performed by using methods based on a time-independent quantum formalism, called ‘close-coupling’ (CC). The quantal formalism has been introduced by Arthurs and Dalgarno [55] for inelastic collisions and then extended to reactive collisions by Schatz & Kuppermann [56].

The three-dimensional time independent quantum mechanical reactive scattering calculations usually employ a method based on body-frame democratic hyperspherical coordinates [57] to represent the nuclear wave function. In the present work, the ABC code [58] and an alternative hyperspherical method [59] have been used to study respectively the dynamics of $\text{H}+\text{H}_2$ and that of the H^++H_2 reaction.

An additional problem that is encountered when dealing with the H_3 and H_3^+ systems is that these are composed by three identical nuclei that are indistinguishable. Contrary to what is usually the case for other reactive systems, the entrance and exit channel cannot be distinguished. H_3 and H_3^+ systems therefore belong to the P_3 nuclear permutation symmetry group and the nuclear wave function, nuclear spin excluded, belong to the $\Gamma = A_2$ or E irreducible representation. The specific symmetry properties of the nuclear wave function can be incorporated in a simple manner, through an appropriate choice of the hyperspherical harmonics that are built from products of simple analytical functions [60].

When the three-particle system under considerations has P_3 permutation symmetry, the nuclear spin of the identical particles must be taken into account. The total nuclear wave function can be written as a direct product of the spatial wave function which satisfies the

spin-independent Schrödinger equation and a nuclear spin wave function. For bosons, the total nuclear wave function is symmetric, whereas, for fermions, it is antisymmetric with respect to interchange of the identical nuclei. Accordingly, for the $\text{H}+\text{H}_2(vj) \rightarrow \text{H}+\text{H}_2(v',j')$ and $\text{H}^++\text{H}_2(v,j) \rightarrow \text{H}^++\text{H}_2(v',j')$ reactions, the physically observable integral cross sections, $\sigma_{vj \rightarrow v'j'}$ that obey the proper spin statistics, can be derived by weighting the calculated integral cross sections [61]:

$$\begin{cases} \sigma_{vj \rightarrow v'j'}^E & j \text{ and } j' \text{ even (para} \rightarrow \text{para)} \\ \frac{2}{3}\sigma_{vj \rightarrow v'j'}^{A_2} + \frac{1}{3}\sigma_{vj \rightarrow v'j'}^E & j \text{ and } j' \text{ odd (ortho} \rightarrow \text{ortho)} \\ \frac{1}{3}\sigma_{vj \rightarrow v'j'}^E & j \text{ odd, } j' \text{ even (ortho} \rightarrow \text{para)} \\ \sigma_{vj \rightarrow v'j'}^E & j \text{ even, } j' \text{ odd (para} \rightarrow \text{ortho)} \end{cases}$$

It is worth mentioning that, if a full quantum method is used to treat the dynamics of three identical nuclei, as in the present work, the reactive and inelastic scattering processes cannot be distinguished.

Alternatively, cross sections may be calculated from wavefunctions which treat the protons as distinguishable by appropriately adding scattering amplitudes for inelastic (e.g., $A+BC \rightarrow A+BC$) and reactive (e. g., $A+BC \rightarrow AB+C$ or $AC+B$) processes obtained from such wavefunctions [62]. In a full description of the collision, the states in the $\text{H}+\text{H}_2$ or H^++H_2 arrangement are described by the quantum numbers j and k (the rotational angular momentum of the H_2 molecule and its projection along the reactant Jacobi vector), and v (the vibrational quantum number of the H_2 molecule). The integral cross section for collision of H or H^+ with $\text{H}_2(v,j)$ to give $\text{H}+\text{H}_2(v',j')$ or $\text{H}^++\text{H}_2(v',j')$, summed over final projection quantum numbers and averaged over initial projection quantum numbers, is given by:

$$\sigma_{vj \rightarrow v'j'}(E_c) = \frac{\pi}{k_{vj}^2(2j+1)} \sum_{Jkk'} (2J+1) |S^J(E, vjk \rightarrow v'j'k')|^2 \quad (1)$$

where k_{vj} denotes the initial wavevector and where the S -matrix for the $\text{H}+\text{H}_2$ or H^++H_2 reaction are given by :

$$\begin{aligned}
|S^J(E, vjk \rightarrow v'j'k')|^2 &= |S_n^J(E, vjk \rightarrow v'j'k') - S_r^J(E, vjk \rightarrow v'j'k')|^2, & j, j' \text{ even} \\
&= |S_n^J(E, vjk \rightarrow v'j'k') + S_r^J(E, vjk \rightarrow v'j'k')|^2 + 2|S_r^J(E, vjk \rightarrow v'j'k')|^2, & j, j' \text{ odd} \\
&= 3|S_r^J(E, vjk \rightarrow v'j'k')|^2, & j \text{ even}, j' \text{ odd} \\
&= |S_r^J(E, vjk \rightarrow v'j'k')|^2, & j \text{ odd}, j' \text{ even}
\end{aligned} \tag{2}$$

S_n^J and S_r^J are the nonreactive and reactive S -matrix elements, respectively.

The summation in Eq. 1 extends over all values of the total angular momentum J which contribute to the reactive or inelastic process. The scattering calculations are carried out on a grid of values of the total energy E . The relevant independent variable for the cross sections is, however, the collision energy E_c , which is the initial translational energy. The two are related by

$$E_{tot} = E_c + \varepsilon_{vj}. \tag{3}$$

where ε_{vj} is the ro-vibrational energy of the H_2 reactant.

From the calculated cross sections $\sigma_{vj \rightarrow v'j'}(E_c)$, one can obtain the corresponding thermal rate coefficients at temperature T by performing a Maxwell-Boltzmann average over the collision energy (E_c):

$$\begin{aligned}
k_{vj \rightarrow v'j'}(T) &= \left(\frac{8}{\pi \mu k_B^3 T^3} \right)^{\frac{1}{2}} \\
&\times \int_0^\infty \sigma_{vj \rightarrow v'j'}(E_c) E_c e^{\frac{-E_c}{k_B T}} dE_c
\end{aligned} \tag{4}$$

where μ is the reduced mass of the reactive system and k_B is the Boltzmann constant.

Note that the quantum mechanical study of the $\text{H}^+ + \text{H}_2$ reaction is more difficult than that of abstraction reactions, such as the $\text{H} + \text{H}_2$ reaction also presented in this review, for two principal reasons. As already mentioned in the previous Section the corresponding PES has a deep well and thus many states have to be taken into account in the close-coupling equations. Moreover, in a such complex forming reaction, symmetric top configurations (where the Coriolis coupling is large) are energetically accessible. All (or nearly all) the allowed Ω components (where Ω is the projection of the total angular momentum J on the axis of least inertia) have to be taken into account in the close-coupling expansion states, in order to obtain accurate cross sections. The maximum value of J , J_{max} , depends on the

maximum of the collision energy employed in the scattering calculations. For the complex-forming $\text{H}^+ + \text{H}_2$ reaction detailed below, the maximum value of the collision energy is 0.1 eV. In this case, $J_{max} = 35$ and Ω varying from 0 to 25 are enough for convergence of integral cross sections. By comparison, converged integral reactive cross sections have been obtained for the $\text{H} + \text{H}_2$ reaction up to 1 eV by using $J_{max} = 75$ and restricting the projection quantum number of J to 6 only. Quantum mechanical calculations using the hyperspherical method described above are therefore very consuming in CPU time and in memory. However, in contrast with the isotopic variant $\text{D}^+ + \text{H}_2$ [53, 54, 63] where the same PES is used, the $\text{H}^+ + \text{H}_2$ system offers a great advantage, the three identical nuclei which noticeably reduce the CPU time. The ABC code and the post-symmetrisation given by Eq. 2 have been used to study the $\text{H} + \text{H}_2$ reaction, while the other TIQM approach has been used to study the $\text{H}^+ + \text{H}_2$ reaction by considering the three nuclei as undistinguishable. Recently, we checked the two methods gave similar results on the $\text{H} + \text{H}_2$ reaction [16]. We showed the equivalence between results obtained by the post-symmetrisation of the S-matrix elements computed using the ABC code and results obtained from S-matrix elements with the correct exchange symmetry (using the other TIQM approach).

We should also mentioned that calculations of the reactive rate constants can be done using quasi-classical trajectory (QCT) method [64, 65]. The QCT method combines the use of classical mechanics, to treat the scattering process, but the quantization of the reactants is taken into account. Quantization is simulated by means of a ‘binning’ procedure, which involves allocating the final states to discrete values of the corresponding quantum numbers. However, the QCT method is only valid as long as the classical mechanics that underpins it. For low temperatures collisions (as those found in the ISM), the QCT approach seems to be not very appropriate because the inability of QCT treatments to conserve the vibrational zero-point energy can render this method unreliable near reaction thresholds.

Accurate statistical methods based on a pure quantum mechanical formalism, such as the statistical quantum mechanical (SQM) method [66, 67], can also be used for the study of complex forming reactions such as the $\text{H}^+ + \text{H}_2$ reaction. An example of such calculations is given in the next section.

III. ORTHO-PARA-H₂ CONVERSION PROCESSES

A. Ortho-para-H₂ conversion by hydrogen exchange

Surprisingly, despite its crucial importance for the physical chemistry of early Universe and of the ISM but also for the physical chemistry of hydrogen plasmas, the OPC process of H₂ due to H collisions has not been the object of many theoretical or experimental investigations. Indeed, in most of the rotationally inelastic excitation studies of H₂ by H, the rigid rotor approximation was used and therefore, the reactive channels were neglected [68, 69]. The goal of these studies was the calculation of rotationally inelastic rate coefficients for astrophysical applications at low to moderate temperatures (below 1000 K). Rigid rotor approach could be justified since the reaction between H and H₂ is inhibited by a large barrier ($\simeq 5000$ K), and the reactive rate constants corresponding to OPC of H₂ are expected to be very small at these temperatures.

The OPC process of H₂ by hydrogen exchange has been already studied by Truhlar [62], Mandy & Martin [70] and by Sun & Dalgarno [71]. The most recent work of Sun & Dalgarno [71], despite relatively accurate, was restricted to p-H₂($j = 0$) and o-H₂($j = 1$) and was then too limited for astrophysical applications of, for example, early Universe. Experimentally, the para-ortho conversion process of H₂ was measured in the temperature range 300-444 K almost 50 years ago by Schulz & Le Roy [72] and to the best of our knowledge, no measurement have been done since then.

The H₃ electronic ground state, on which the H + H₂ dynamical calculations are performed conically intersects the first excited state [73]. The crossing occurs at an energy of 2.7 eV with respect to the bottom of the H₂ ground electronic states well. As a consequence, there is a sign change of the electronic wavefunction as one follows a closed path in nuclear configuration space around the line of the conical intersection. This sign change is usually referred as the geometric phase effect which can be globally taken into account at low energies ($E < 15000$ cm⁻¹) by reversing the sign of the S_r^J [74, 75] matrices using the theoretical approach which treat the protons as distinguishable. The geometric phase effect has been discussed in detail in reviews of Aoiz et al. [76] and Bouakline et al. [73]

Apart from the geometric phase effects, non-adiabatic transitions in the region of proximity of the two electronic surfaces are also possible (at high collision energies). However,

for these systems, it has been found that non-adiabatic transitions are unlikely to occur [73]. Then, $\text{H} + \text{H}_2$ reaction can be safely studied within the Born-Oppenheimer approximation contrarily to what has been found for others simple reactions such as $\text{F} + \text{H}_2$ [77, 78] or $\text{Cl} + \text{H}_2$ [79].

Recently, we investigated the OPC process of H_2 by hydrogen exchange [16] (hereafter Paper I) within the Born-Oppenheimer approximation. In our investigation of the scattering dynamics, we used the H_3 global potential energy surface (PES) of Mielke *et al.* [47] that was proved to be very successful in the calculation of $\text{H} + \text{H}_2$ thermal rate coefficients [80]. We used a pure quantum time independent approach in order to get a very accurate modeling of this crucial process for the astrophysical modeling of “hot” environment and of early Universe. In these calculations, we considered results only for H_2 molecules in their ground vibrational states (despite excited vibrational levels were included in the calculations) and we considered transitions between rotational states up to $j = 10$.

First of all, in Paper I, we checked that, at low and intermediate collisional energies, the geometric phase effect can be neglected. Nevertheless, all results were obtained including the geometric phase effect (by reversing the sign of the S_r^J).

In Paper I, we have computed the collisional energy dependence of the inelastic and reactive cross sections (considering the particle as distinguishable) and we get the cross sections for the rotational excitation of H_2 by H using the post-symmetrisation described above. Figure 2 displays the energy dependence of the calculated integral cross sections for rotational (de-)excitation of p- and o- H_2 by H , respectively.

As already discussed in Paper I, at low collisional energies, the magnitude of the p-o- H_2 and o-p- H_2 cross sections is small and in any case, these cross sections are much smaller than those for transitions conserving the nuclear spin ($\Delta j = 2$). OPC process of H_2 is then relatively negligible at low energies compared to the pure rotational excitation process. It is interesting to note that, at the opposite of what has been found for the same H_2 transition due to H^+ collisions (see below), the de-excitation $\text{H} + \text{o-}\text{H}_2(j = 1) \rightarrow \text{H} + \text{p-}\text{H}_2(j = 0)$ cross sections is negligibly small at low collisional energies even if it is the only energetically possible process. These results were expected and could have been anticipated. Indeed, as the reaction proceeds by tunneling effect, the magnitude of the cross sections is negligible at these low energies.

However, the magnitude of the cross sections increases rapidly with increasing collisional

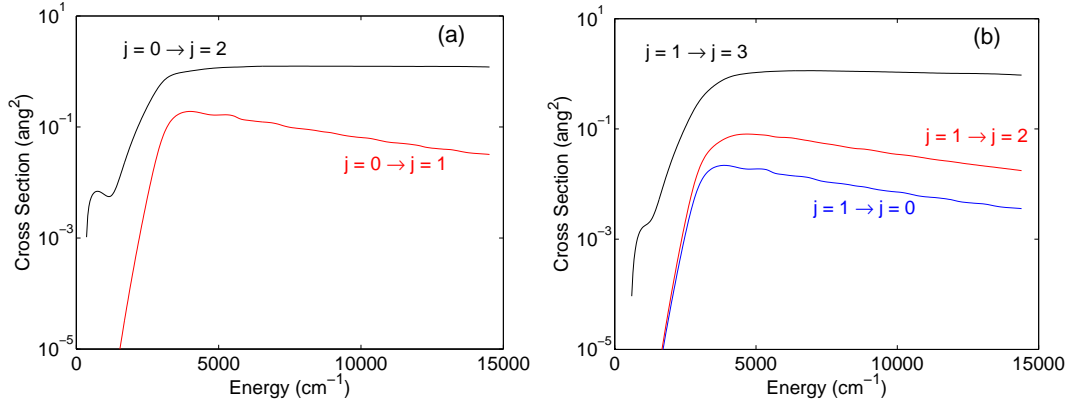


FIG. 2: Collision energy dependence of the integral cross section for the rotational excitation of $p\text{-H}_2(j=0)$ (a) and $o\text{-H}_2(j=1)$ (b) by H. Reprinted with permission from Ref. [16]. Copyright 2012 American Institute of Physics.

energies and at collisional energy $\sim 2000\text{--}3000\text{ cm}^{-1}$, the spin conversion process becomes only one order of magnitude smaller than the spin conserving process, showing the clear competition between inelastic and reactive processes.

Taking into account the relatively large abundance of hydrogen atom in diffuse ISM or in early Universe, the OPC process of H_2 by hydrogen exchange remains a major process in the OPC process of H_2 as soon as these collisional energies are encountered. The temperature variation of the corresponding rate coefficients have been computed from the inelastic cross sections (Paper I).

Figure 3 presents the temperature dependence of the rate coefficients corresponding to the cross sections presented in Fig. 2. As expected, the OPC processes are not negligible above $\sim 300\text{ K}$ and will start to play a role in the thermalization of the OPR of H_2 in media with temperature greater than 300 K . State to state $\text{H}+\text{H}_2$ rate constants between the first eleven levels of $\text{H}_2(j=0-10)$ are given in Tables I and II for temperatures equal to 10, 20, 30, 50, 100, 200, 300, 500, 700, 1000 and 1500 K.

The new theoretical results have then been compared with previous experimental results. Figure 4 present a comparison of the theoretical results (properly averaged over H_2 rotational distribution) (see Paper I) with the experimental ones of Schulz & Le Roy [72]. The agreement with experimental results [72] is a new nice illustration of the detailed understanding of the simplest chemical reaction.

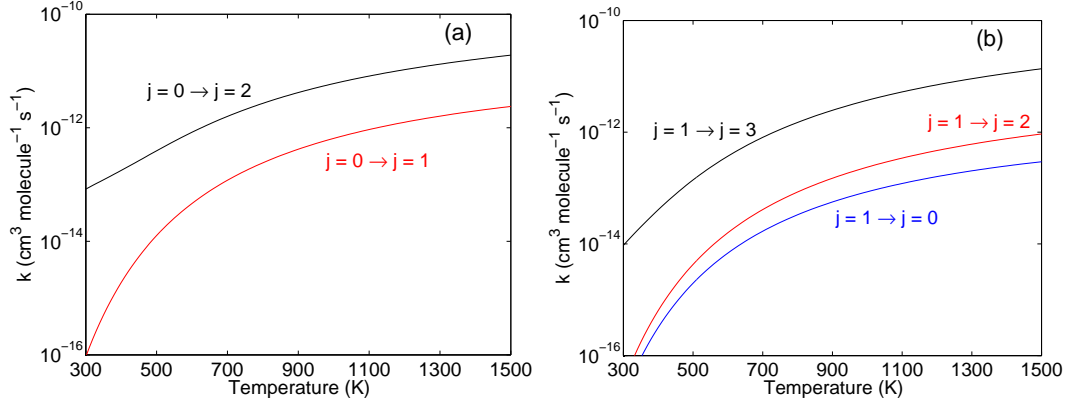


FIG. 3: Temperature dependence of the rate coefficients for the rotational excitation of p-H₂ (a) and o-H₂ (b) by H. Reprinted with permission from Ref. [16]. Copyright 2012 American Institute of Physics.

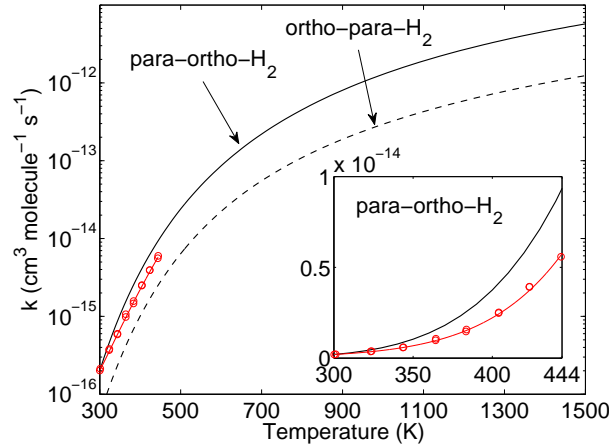


FIG. 4: Temperature dependence of the rate coefficients for the para-ortho-H₂ and ortho-para-H₂ conversion. The line with circles indicates the experimental results of Schulz and Le Roy [72]. Reprinted with permission from Ref. [16]. Copyright 2012 American Institute of Physics.

The new rotational rate constants were also compared with the previously available data of Sun & Dalgarno [71] also calculated using a quantum time-independent approach. The present data differ from the previous results especially at low temperature (see Paper I). The differences are a signature of the different H₃ PES used in the two calculations. Sun & Dalgarno [71] used the DMBE [44] PES whereas we used the most recent PES of Mielke *et al.* [47]. Then, we recommend the use of the new rate constants for the astrophysical

TABLE I: State to state $\text{H}_2 + \text{H}$ rate constants. The rates are in units of $\text{cm}^3 \text{s}^{-1}$.

j	j'	10K	20K	30K	50K	100K	200K	300K	500K	700K	1000	1500K
1	0	1.24(-24)	2.10(-24)	3.29(-24)	8.98(-24)	2.17(-22)	1.56(-19)	1.82(-17)	1.98(-15)	1.69(-14)	8.57(-14)	2.96(-13)
2	0	6.02(-14)	6.37(-14)	6.37(-14)	6.44(-14)	7.02(-14)	8.01(-14)	9.16(-14)	2.19(-13)	6.59(-13)	2.00(-12)	5.35(-12)
2	1	8.21(-23)	9.67(-23)	1.18(-22)	2.37(-22)	3.99(-21)	2.07(-18)	1.82(-16)	1.52(-14)	1.20(-13)	5.98(-13)	2.10(-12)
3	0	2.33(-22)	3.13(-22)	4.02(-22)	7.25(-22)	5.88(-21)	1.04(-18)	5.01(-17)	2.46(-15)	1.59(-14)	7.02(-14)	2.30(-13)
3	1	8.11(-15)	1.06(-14)	1.26(-14)	1.62(-14)	2.49(-14)	4.04(-14)	6.75(-14)	3.25(-13)	1.16(-12)	3.72(-12)	1.03(-11)
3	2	7.19(-23)	1.02(-22)	1.40(-22)	3.03(-22)	4.35(-21)	1.60(-18)	9.76(-17)	6.20(-15)	4.69(-14)	2.37(-13)	8.76(-13)
4	0	1.29(-17)	1.81(-17)	2.31(-17)	3.58(-17)	1.01(-16)	6.03(-16)	2.89(-15)	3.12(-14)	1.26(-13)	4.42(-13)	1.27(-12)
4	1	1.08(-20)	1.48(-20)	1.99(-20)	3.64(-20)	2.44(-19)	2.34(-17)	6.39(-16)	2.04(-14)	1.19(-13)	5.14(-13)	1.72(-12)
4	2	1.74(-16)	2.95(-16)	4.40(-16)	8.41(-16)	2.83(-15)	1.59(-14)	6.05(-14)	4.07(-13)	1.35(-12)	4.01(-12)	1.06(-11)
4	3	4.86(-22)	7.71(-22)	1.13(-21)	2.54(-21)	3.31(-20)	8.14(-18)	3.39(-16)	1.77(-14)	1.33(-13)	7.01(-13)	2.76(-12)
5	0	2.09(-20)	2.94(-20)	3.81(-20)	6.43(-20)	3.26(-19)	1.26(-17)	1.61(-16)	2.88(-15)	1.43(-14)	5.73(-14)	1.86(-13)
5	1	3.27(-17)	4.45(-17)	5.49(-17)	7.92(-17)	1.93(-16)	1.18(-15)	6.69(-15)	7.91(-14)	3.41(-13)	1.22(-12)	3.67(-12)
5	2	2.34(-20)	3.35(-20)	4.43(-20)	7.83(-20)	4.61(-19)	2.39(-17)	3.88(-16)	9.23(-15)	5.18(-14)	2.25(-13)	7.82(-13)
5	3	1.26(-15)	1.73(-15)	2.17(-15)	3.20(-15)	7.75(-15)	3.36(-14)	1.06(-13)	5.66(-13)	1.72(-12)	4.99(-12)	1.33(-11)
5	4	3.90(-22)	6.05(-22)	8.71(-22)	1.89(-21)	2.17(-20)	3.39(-18)	1.07(-16)	5.03(-15)	3.86(-14)	2.13(-13)	8.97(-13)
6	0	1.38(-17)	1.17(-17)	9.85(-18)	8.66(-18)	1.70(-17)	1.87(-16)	1.30(-15)	1.52(-14)	6.26(-14)	2.12(-13)	6.02(-13)
6	1	7.27(-18)	6.24(-18)	5.32(-18)	4.98(-18)	1.31(-17)	2.06(-16)	1.63(-15)	2.34(-14)	1.12(-13)	4.43(-13)	1.45(-12)
6	2	2.90(-16)	2.49(-16)	2.11(-16)	1.85(-16)	2.98(-16)	1.67(-15)	8.16(-15)	7.94(-14)	3.19(-13)	1.10(-12)	3.22(-12)
6	3	1.83(-18)	1.59(-18)	1.39(-18)	1.40(-18)	4.71(-18)	1.24(-16)	1.47(-15)	3.01(-14)	1.68(-13)	7.45(-13)	2.68(-12)
6	4	1.81(-14)	1.55(-14)	1.32(-14)	1.14(-14)	1.60(-14)	5.23(-14)	1.46(-13)	6.62(-13)	1.82(-12)	4.83(-12)	1.20(-11)
6	5	1.13(-20)	1.01(-20)	9.39(-21)	1.18(-20)	9.17(-20)	1.01(-17)	2.78(-16)	1.26(-14)	9.93(-14)	5.75(-13)	2.55(-12)
7	0	7.12(-19)	9.71(-19)	1.20(-18)	1.79(-18)	4.98(-18)	3.95(-17)	2.42(-16)	2.87(-15)	1.26(-14)	4.71(-14)	1.50(-13)
7	1	1.17(-17)	1.62(-17)	2.03(-17)	3.07(-17)	9.04(-17)	7.73(-16)	4.61(-15)	5.13(-14)	2.14(-13)	7.54(-13)	2.25(-12)
7	2	1.42(-18)	1.97(-18)	2.47(-18)	3.79(-18)	1.20(-17)	1.22(-16)	8.24(-16)	1.11(-14)	5.25(-14)	2.08(-13)	6.90(-13)
7	3	5.50(-17)	7.55(-17)	9.37(-17)	1.37(-16)	3.46(-16)	2.18(-15)	1.09(-14)	1.09(-13)	4.58(-13)	1.67(-12)	5.21(-12)
7	4	2.07(-19)	2.95(-19)	3.84(-19)	6.40(-19)	2.71(-18)	5.20(-17)	5.23(-16)	1.01(-14)	5.70(-14)	2.59(-13)	9.60(-13)
7	5	3.27(-15)	4.47(-15)	5.49(-15)	7.72(-15)	1.64(-14)	5.91(-14)	1.64(-13)	7.31(-13)	2.01(-12)	5.45(-12)	1.41(-11)
7	6	8.63(-22)	1.31(-21)	1.85(-21)	3.79(-21)	3.46(-20)	3.18(-18)	8.09(-17)	3.60(-15)	2.91(-14)	1.74(-13)	8.08(-13)
8	0	4.99(-18)	6.23(-18)	7.27(-18)	1.00(-17)	2.65(-17)	2.01(-16)	1.09(-15)	1.07(-14)	4.16(-14)	1.33(-13)	3.67(-13)
8	1	8.18(-18)	1.03(-17)	1.21(-17)	1.70(-17)	4.61(-17)	3.71(-16)	2.14(-15)	2.35(-14)	9.99(-14)	3.68(-13)	1.17(-12)
8	2	1.95(-17)	2.44(-17)	2.85(-17)	3.96(-17)	1.05(-16)	7.92(-16)	4.40(-15)	4.54(-14)	1.82(-13)	6.18(-13)	1.78(-12)
8	3	7.69(-18)	9.82(-18)	1.17(-17)	1.69(-17)	4.95(-17)	4.55(-16)	3.02(-15)	4.06(-14)	1.91(-13)	7.52(-13)	2.51(-12)
8	4	7.28(-17)	9.27(-17)	1.10(-16)	1.53(-16)	3.77(-16)	2.25(-15)	1.03(-14)	9.03(-14)	3.51(-13)	1.20(-12)	3.57(-12)
8	5	1.13(-18)	1.47(-18)	1.80(-18)	2.80(-18)	1.07(-17)	1.73(-16)	1.62(-15)	3.08(-14)	1.75(-13)	8.03(-13)	3.01(-12)
8	6	3.77(-15)	4.81(-15)	5.66(-15)	7.64(-15)	1.60(-14)	5.82(-14)	1.64(-13)	7.26(-13)	1.94(-12)	5.00(-12)	1.22(-11)
8	7	5.21(-21)	6.96(-21)	8.92(-21)	1.61(-20)	1.25(-19)	9.56(-18)	2.27(-16)	9.79(-15)	7.97(-14)	4.87(-13)	2.31(-12)

modeling.

Finally, it was interesting to compare the results of purely rotationally inelastic scattering of H_2 by H using the rigid rotor approximation and neglecting the reactive channels with the results of Paper I. Indeed, as mentioned above, most of the work dealing with the collisional

TABLE II: $\text{H}_2 + \text{H}$ rate constants. The rates are in units of $\text{cm}^3 \text{s}^{-1}$.

j	j'	10K	20K	30K	50K	100K	200K	300K	500K	700K	1000	1500K
9	0	6.59(-19)	1.04(-18)	1.42(-18)	2.32(-18)	6.76(-18)	4.88(-17)	2.56(-16)	2.51(-15)	1.01(-14)	3.57(-14)	1.12(-13)
9	1	1.06(-17)	1.65(-17)	2.23(-17)	3.63(-17)	1.07(-16)	8.07(-16)	4.30(-15)	4.17(-14)	1.62(-13)	5.38(-13)	1.55(-12)
9	2	2.13(-18)	3.37(-18)	4.63(-18)	7.75(-18)	2.42(-17)	2.00(-16)	1.13(-15)	1.18(-14)	4.92(-14)	1.77(-13)	5.58(-13)
9	3	1.51(-17)	2.36(-17)	3.22(-17)	5.33(-17)	1.63(-16)	1.32(-15)	7.52(-15)	7.99(-14)	3.29(-13)	1.16(-12)	3.50(-12)
9	4	1.57(-18)	2.45(-18)	3.35(-18)	5.59(-18)	1.83(-17)	1.77(-16)	1.20(-15)	1.60(-14)	7.38(-14)	2.85(-13)	9.33(-13)
9	5	4.63(-17)	7.15(-17)	9.63(-17)	1.55(-16)	4.34(-16)	2.78(-15)	1.34(-14)	1.26(-13)	5.14(-13)	1.83(-12)	5.65(-12)
9	6	2.20(-19)	3.90(-19)	5.78(-19)	1.08(-18)	4.36(-18)	6.38(-17)	5.68(-16)	1.07(-14)	6.05(-14)	2.75(-13)	1.02(-12)
9	7	1.86(-15)	2.80(-15)	3.69(-15)	5.67(-15)	1.33(-14)	5.24(-14)	1.53(-13)	7.08(-13)	1.95(-12)	5.20(-12)	1.32(-11)
9	8	4.39(-21)	5.28(-21)	5.79(-21)	8.14(-21)	5.59(-20)	3.59(-18)	7.79(-17)	3.10(-15)	2.47(-14)	1.50(-13)	7.06(-13)
10	0	4.82(-18)	6.29(-18)	7.43(-18)	1.02(-17)	2.66(-17)	1.97(-16)	1.02(-15)	9.02(-15)	3.19(-14)	9.55(-14)	2.45(-13)
10	1	1.08(-17)	1.43(-17)	1.68(-17)	2.29(-17)	5.87(-17)	4.24(-16)	2.19(-15)	2.04(-14)	7.89(-14)	2.71(-13)	8.26(-13)
10	2	1.99(-17)	2.57(-17)	3.01(-17)	4.05(-17)	1.03(-16)	7.51(-16)	3.93(-15)	3.65(-14)	1.35(-13)	4.27(-13)	1.16(-12)
10	3	2.03(-17)	2.63(-17)	3.08(-17)	4.18(-17)	1.09(-16)	8.42(-16)	4.59(-15)	4.65(-14)	1.87(-13)	6.54(-13)	1.99(-12)
10	4	2.25(-17)	2.95(-17)	3.52(-17)	4.89(-17)	1.31(-16)	9.99(-16)	5.37(-15)	5.29(-14)	2.08(-13)	7.02(-13)	2.02(-12)
10	5	9.40(-18)	1.25(-17)	1.50(-17)	2.16(-17)	6.42(-17)	6.39(-16)	4.34(-15)	5.59(-14)	2.50(-13)	9.36(-13)	2.94(-12)
10	6	9.28(-17)	1.21(-16)	1.43(-16)	1.95(-16)	4.79(-16)	2.98(-15)	1.33(-14)	1.08(-13)	3.92(-13)	1.26(-12)	3.54(-12)
10	7	2.17(-18)	2.86(-18)	3.45(-18)	5.02(-18)	1.67(-17)	2.18(-16)	1.83(-15)	3.38(-14)	1.88(-13)	8.36(-13)	2.98(-12)
10	8	2.42(-15)	3.19(-15)	3.80(-15)	5.14(-15)	1.12(-14)	4.53(-14)	1.36(-13)	6.34(-13)	1.69(-12)	4.24(-12)	9.88(-12)
10	9	9.59(-21)	1.00(-20)	1.17(-20)	2.62(-20)	2.55(-19)	1.46(-17)	2.64(-16)	8.89(-15)	6.80(-14)	4.02(-13)	1.84(-12)

excitation of H_2 by H has been performed using these approximation. In such approximation, the OPC process of H_2 is neglected.

Then, we have performed calculations for pure rotational excitation of H_2 by H using the rigid rotor approximation. We have chosen for the H_2 internuclear separation $r_{\text{H}_2} = 1.449 \text{ a}_0$, the ground state vibrationally averaged value. The standard time-independent coupled scattering equations were solved using the MOLSCAT code [81].

Figures 5 displays the energy dependence of the calculated integral cross sections for rotational excitation obtained using a rigid rotor approximation and obtained from a full 3D approach that include the reactive channels.

One can see that the 2D approach leads to results in moderate agreement with those of the 3D approach, the agreement being better for small Δj transitions than for larger Δj transitions. This reflects the fact that transitions with large Δj , which have the smallest cross sections, are the most sensitive to modest changes in the PES.

At low collisional energies, just above the thresholds, the 2D and 3D results are in reasonable agreement (especially for $\Delta j = 2$ transitions). This could have been anticipated since the reactive process, that could disturb the pure rotational excitation, is inhibited by

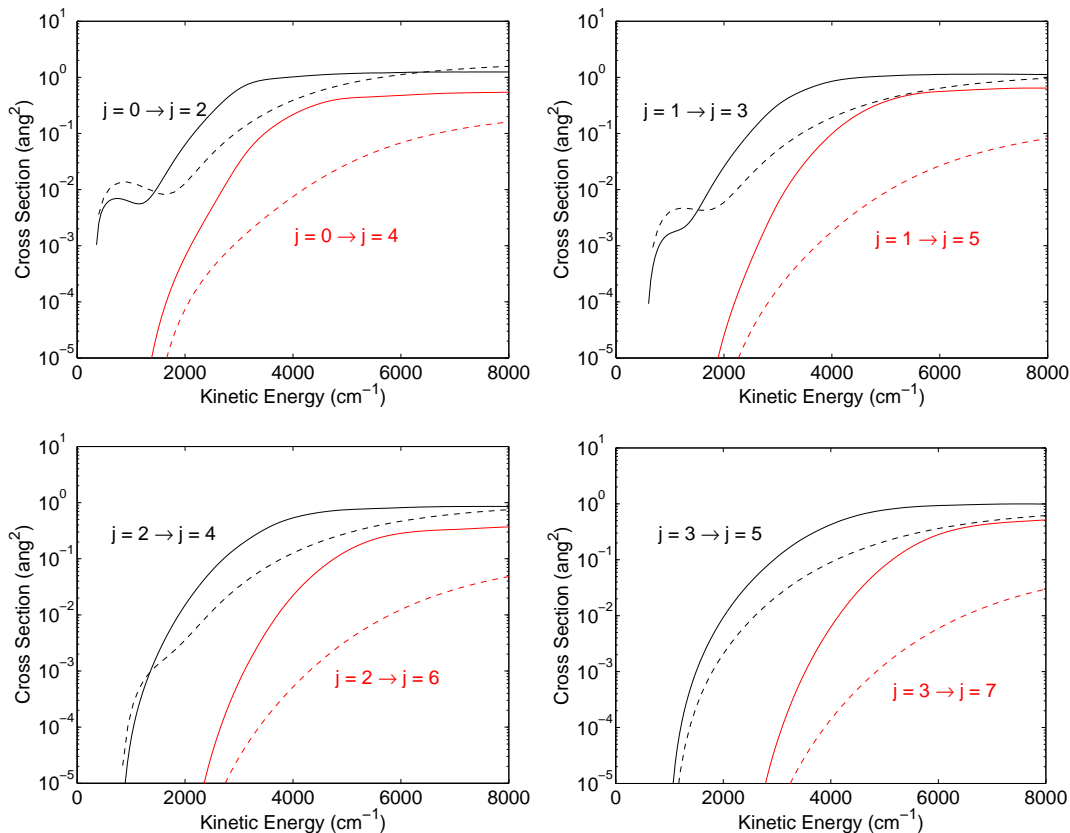


FIG. 5: Collision energy dependence of the integral cross section for the rotational excitation of para- $\text{H}_2(j = 0, 2)$ and ortho- $\text{H}_2(j = 1, 3)$ by H. The solid lines correspond to exact 3D results. The dashed lines correspond to 2D results.

the reaction barrier.

However, both sets of results rapidly disagree with increasing energy despite the collisional energy is still largely lower the barrier height.

Two obvious reasons can explain these differences :

- (i) The 2D approach does not take into account the vibration of H_2 in the scattering calculations.
- (ii) The 2D approach neglects the reactive channels.

At these intermediate collisional energies (where the reactants have not enough energy to overcome the barrier), one could have expected that the 2D approach, which entirely neglects the reactive OPC process of H_2 , would overestimate the purely inelastic process. However, the opposite behaviour is found. As a result, the deviation between the two sets of cross sections cannot be explained by the presence of the (closed) reactive channels. Such

behaviour was already observed for the rotational excitation of D_2 by H also performed using rigid rotor approximation and full 3D approach [82].

In fact, the behaviour with collision energy and the magnitudes of the 2D and 3D inelastic cross sections can be related to the radial dependence of the (intermolecular) potential expansion coefficients $v_i(R)$. Wrathmall & Flower [69] found in their study on the rotational excitation of H_2 by H, using the PES of Mielke *et al.* [47], that the cross section for the $j = 0 \rightarrow j' = 2$ transition significantly decreases at moderate energies due to the shape of the $v_2(R)$ expansion coefficient. The present cross sections follow exactly the same behaviour. Wrathmall & Flower [69] also found that the minima in the cross sections were lowered and shifted to lower energies when the expansion coefficients were averaged over the vibrational ground state wave function (instead of fixing the internuclear separation at its equilibrium value). Hence the difference between the present 2D and 3D results at moderate energies certainly reflects these intramolecular effects and shows the importance of using 3D potential energy surfaces.

At high kinetic energies (above $\sim 5000 \text{ cm}^{-1}$), the 2D cross sections tend to converge towards the 3D cross sections. However, at even higher kinetic energies, the 2D results can exceed the actual (3D) cross sections, as observed in Fig. 5 for the $j = 0 \rightarrow 2$ transition above $\sim 6000 \text{ cm}^{-1}$. This behaviour is expected in this energy regime since the scattering flux is directed into both inelastic and reactive channels. On the other hand, as observed in Fig. 2, the reactive cross sections ($\Delta j = 1$) are significantly smaller than the purely inelastic ones. This explains why the 2D and 3D results are in rather good agreement in the high energy regime, in spite of the opening of the reactive channels. In summary, the major 3D effects occur at intermediate energies (in the range $\sim 2000 - 6000 \text{ cm}^{-1}$) and are caused by the intramolecular dependence of the PES expansion coefficients.

We conclude that the calculations of rotationally inelastic rate coefficients using the 2D approach provide the correct order of magnitude for the dominant transitions ($\Delta j = 2$) but the 3D approach is necessary for an accuracy at the state-to-state level better than a factor of ~ 3 . We also recommend the use of our new data for modeling the pure rotational excitation process of H_2 by H.

B. Ortho–para-H₂ conversion by proton exchange

The reaction with H, presented just above, has a substantial activation energy (~ 5000 K) and it is thus inefficient at low temperatures as those found for instance in the interstellar dense clouds (about 10 K). The same happens for reaction with H₂. As a result, collisions of H₂ with protons, H⁺, are expected to drive the OPR of H₂ in most cold astrophysical environments, from the primordial to the interstellar gas. The knowledge of the rate coefficients for the H⁺+H₂ reaction, especially for the $j = 1 \rightarrow j' = 0$ transition, is thus of fundamental interest, and especially for the cold astrophysical media. Given the very low population of the rotationally excited H₂ below 100 K, we consider here only the $j = 0$ and $j = 1$ rotational states of H₂.

Like the H+H₂ reaction, the H⁺+H₂ reaction is one of the simplest elementary reaction and, surprisingly, there exist only approximate calculations for the OPC process of H₂. The current astrophysical models use values of the rate coefficients that have been computed 20 years ago by Gerlich [83] using a statistical approach. Recently, we have computed for the first time the rate coefficients for the OPC of H₂ by proton exchange at low temperature ($T < 100$ K) with a high accuracy [17, 19]. The fully time independent quantum mechanical (TIQM) method combined with the most recent global *ab initio* PES, both being described above, was employed. We therefore used the same PES and the same TIQM method than for the study of the D⁺+H₂ for which an excellent agreement has been obtained between the theoretical results and the measurements [54]. Statistical quantum mechanical (SQM) [66, 67] calculations were also performed for the H⁺+H₂ reaction and its isotopic variants [17–19, 84, 85]. The SQM approach is based on the assumption that the process takes place *via* a complex-forming mechanism and that seems to be justified in the H⁺+H₂ reaction. A comparison between the SQM and the TIQM results could confirm or not the statistical behaviour of H⁺+H₂. The considerations mentioned above for symmetries and nuclear spin also apply to the SQM method which is also based on a quantum mechanical formalism.

We were interested in collision energies up to 0.1 eV, and thus the charge transfer channel leading to H₂⁺+H is not accessible (open at 1.8 eV). However, we have to mention that non-adiabatic interaction with the charge transfer channel could modify the energy level spectrum of H₃⁺ and it might influence the dynamics. However, as for the H + H₂ reaction, we expect that these non-adiabatic process may not be very important, justifying the Born-

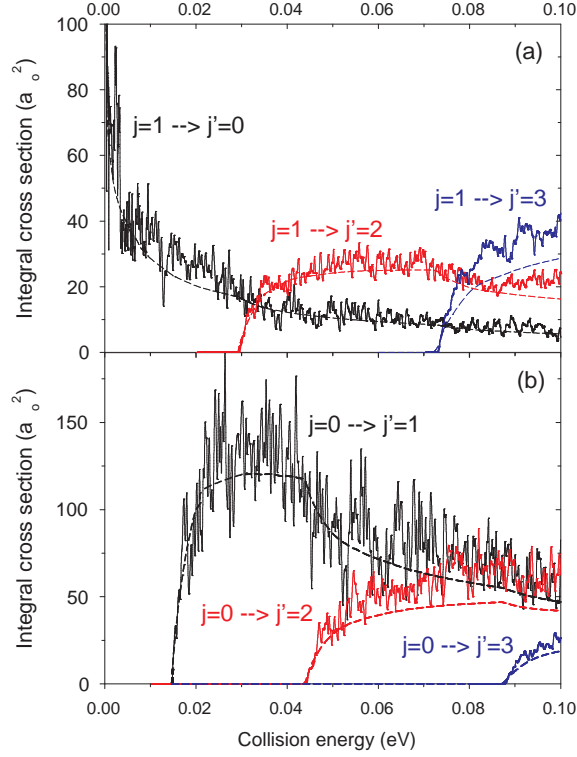


FIG. 6: TIQM (solid line) and SQM (dashed line) integral cross sections as a function of the collision energy for $\text{H}^+ + \text{H}_2(v = 0, j = 1) \rightarrow \text{H}^+ + \text{H}_2(v = 0, j')$ (a) and $\text{H}^+ + \text{H}_2(v = 0, j = 0) \rightarrow \text{H}^+ + \text{H}_2(v = 0, j')$ (b). Reprinted with permission from Ref. [17]. Copyright 2011 American Physical Society.

Oppenheimer approximation that was used. In addition, considering the temperature range chosen in this study ($T < 100$ K), only the fundamental vibrational quantum number $v = 0$ of H_2 is considered.

Fig. 6a shows the TIQM cross sections for the $\text{H}^+ + \text{H}_2(v = 0, j = 1) \rightarrow \text{H}^+ + \text{H}_2(v = 0, j')$ reaction. As expected for a barrierless entrance channel, the cross sections for the $j = 1 \rightarrow j' = 0$ OPC process of H_2 decreases relatively smoothly with the collision energy. There is indeed no energy threshold, in contrast with the case of the $j = 1 \rightarrow j' = 2$ and $j = 1 \rightarrow j' = 3$ transitions where energy thresholds of 0.029 eV and 0.073 eV respectively exist. These values correspond to the energy difference between the rotational levels involved in these transitions. The main result shown in Fig. 6a is that the OPC of H_2 , $j = 1 \rightarrow j' = 0$, is the only possible process at the lowest collision energies. Another interesting feature is

the resonance structure found in the cross sections. These resonances, which have survived to the partial wave J summation, average the more narrow peaks observed in the reaction probabilities (not shown here), which are linked to the presence of a long-lived intermediate complex, H_3^+ , formed in the deep well (4.6 eV) of the PES which supports many quasi-bound states. A recent experimental study [86] has shown that the observed resonances here can be directly related with H^+-H_2 radiative association processes.

The situation is totally different for the $\text{H} + \text{H}_2$ reaction where no resonance structure was found (see for instance Fig 2) because of the existence of a very short-lived H_3 complex during the collision. The SQM method by nature cannot reproduce the numerous peaks. However, on average, a fairly good agreement is obtained in average for all processes.

TIQM cross sections for the $\text{H}^+ + \text{H}_2(v = 0, j = 0) \rightarrow \text{H}^+ + \text{H}_2(v = 0, j')$ reaction are presented in Fig. 6b. In contrast with the previous processes, an energy threshold is observed here for all transitions because the reaction is always endothermic. Many resonances are found again and the SQM prediction is in good agreement with the TIQM results. By combining the agreement found also for the $j = 1 \rightarrow j'$, it is clear that the $\text{H}^+ + \text{H}_2$ reaction is statistical at low collision energies. In conclusion, the only possible transition at very low collision energies (below 0.015 eV) is the $j = 1 \rightarrow j' = 0$ OPC process of H_2 , while at higher collision energies the $j = 0 \rightarrow j' = 1$ process is dominant.

Fig. 7a displays the TIQM rate coefficients calculated from the cross sections for the $\text{H}^+ + \text{H}_2(v = 0, j = 1) \rightarrow \text{H}^+ + \text{H}_2(v = 0, j')$ reaction for temperatures up to 100 K. These rate coefficients have been obtained by integration of the cross sections shown in Fig. 6a using a Maxwell-Boltzmann distribution over the collision energies. As expected from the absence of energy threshold in the cross sections for the $\text{H}^+ + \text{H}_2(v = 0, j = 1) \rightarrow \text{H}^+ + \text{H}_2(v = 0, j' = 0)$ reaction, the OPC process of H_2 , $j = 1 \rightarrow j' = 0$, is the dominant process at low temperature. The rate coefficient is almost independent of temperature with a constant value of about $1.5 \cdot 10^{-10} \text{ cm}^3 \cdot \text{molecule}^{-1} \cdot \text{s}^{-1}$, which is about 1/17 of the (temperature independent) Langevin rate value ($2.5 \cdot 10^{-9} \text{ cm}^3 \cdot \text{molecule}^{-1} \cdot \text{s}^{-1}$). The two other rate coefficients for the $j = 1 \rightarrow j' = 2$ and $j = 1 \rightarrow j' = 3$ transitions increase steadily with temperature with changes of some order of magnitudes. They follow the same order than that found for the cross sections, and still remain much lower than the rate for $j = 1 \rightarrow j' = 0$.

Following the good agreement in average between the SQM and TIQM cross sections, the SQM rate coefficients are also in good agreement with the TIQM prediction. This

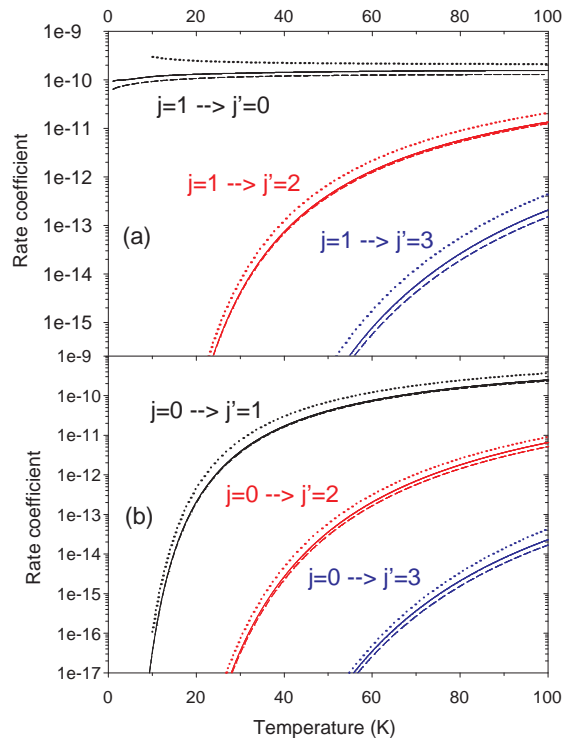


FIG. 7: TIQM (solid line), SQM (dashed line) and SM (dotted line) rate coefficients (in $\text{cm}^3.\text{molecule}^{-1}.\text{s}^{-1}$) as a function of the temperature for $\text{H}^+ + \text{H}_2(v = 0, j = 1) \rightarrow \text{H}^+ + \text{H}_2(v = 0, j')$ (a) and $\text{H}^+ + \text{H}_2(v = 0, j = 0) \rightarrow \text{H}^+ + \text{H}_2(v = 0, j')$ (b). Reprinted with permission from Ref. [19]. Copyright 2012 American Physical Society.

comparison and the previous ones allow to unambiguously establish the statistical nature of the reaction at low temperature. Nevertheless, it is worth mentioning nevertheless that this work focusses entirely on state-to-state quantities, which, in principle, constitute the most severe test for a statistical technique. The agreement with the corresponding exact quantum mechanical rate coefficients for $T > 10$ K is therefore a remarkable result.

The rate coefficients computed from another statistical model (SM) developed by Gerlich [83], more simple than the SQM method, are also shown. These rates follow the general trends of the TIQM and SQM rate coefficients. However, some differences exist. First, for the $j = 1 \rightarrow j' = 0$ OPC process of H_2 , the dependence on temperature for the SM rate coefficient at the lowest temperatures (below 30 K) is reverse of that found by the SQM and TIQM methods. Second, for all transitions and for the whole temperature range considered

TABLE III: Parameters for the fits of the TIQM rate coefficients to the Kooij analytical expression $k(T) = \alpha(T/300)^\beta \exp(-\gamma/T)$ for the different $\text{H}^+ + \text{H}_2(v = 0, j) \rightarrow \text{H}^+ + \text{H}_2(v' = 0, j')$ reactions (indicated as $j \rightarrow j'$ in the table). α is measured in $\text{cm}^3 \text{ molecule}^{-1} \text{ s}^{-1}$ and γ in K. Parenthesis (x) stand for 10^x . Temperature range at which the proposed fitting expressions yield errors below $\sim 5\%$ are listed at the last line. Reprinted with permission from Ref. [18]. Copyright 2011 Royal Society of Chemistry.

	$0 \rightarrow 1$	$0 \rightarrow 2$	$0 \rightarrow 3$	$1 \rightarrow 0$	$1 \rightarrow 2$	$1 \rightarrow 3$
α	1.490(-9)	1.185(-9)	2.526(-10)	1.823(-10)	0.434(-9)	0.706(-9)
β	2(-4)	-0.0168	-1.3214	0.1289	0.0030	-0.7877
γ	178.25	522.0667	1075.3996	-0.0214	346.8679	899.4216
T range (K)	20-100	30-100	40-100	10-100	10-100	50-100

here, the SM rate coefficient always overestimates the SQM and TIQM rate coefficients.

Astrophysical models, including the *ortho-para* distinction of H_2 , may present significant effects relatively to these differences found between the different computed rate coefficients, especially for the $j = 1 \rightarrow j' = 0$ OPC process of H_2 . We thus encourage the astrophysicists to use in their future models the TIQM rate coefficients which are as accurate as possible and constitute a valid benchmark.

The TIQM rate coefficients for the $\text{H}^+ + \text{H}_2(v = 0, j = 0) \rightarrow \text{H}^+ + \text{H}_2(v = 0, j')$ are displayed in Fig. 7b for temperatures up to 100 K. The main comments mentioned above apply here again. The comparison between Fig. 7a and Fig. 7b definitively confirms that the OPC process of H_2 , $j = 1 \rightarrow j' = 0$, is the main process for temperatures below 50 K. Above this temperature, the $j = 0 \rightarrow j' = 1$ para-ortho conversion process becomes also important.

Given their importance for interstellar models and for practical purposes, fits of the TIQM rate coefficients between $T = 10$ K and $T = 100$ K for the state-to-state $\text{H}^+ + \text{H}_2(v = 0, j = 0, 1) \rightarrow \text{H}^+ + \text{H}_2(v' = 0, j')$ reactions to the analytical Kooij formula, $k(T) = \alpha(T/300)^\beta \exp(-\gamma/T)$, have been performed. Values for the corresponding parameters are shown in Table III.

IV. DISCUSSION AND ASTROPHYSICAL APPLICATIONS

As discussed in the introduction, molecular hydrogen is the most abundant molecule in the Universe and its OPR plays a fundamental role in both the physics and chemistry of the ISM and of the early universe. In this section we discuss the relative role of the different OPC processes, that is *via* reactive collisions with hydrogenated species (H , H^+ , H_2 , H_3^+) and *via* interaction with solid surfaces. In the cold ISM ($T \sim 10 \text{ K}$), only H^+ , H_3^+ and the icy dust grains can contribute to the OPC of H_2 because of the large energy barriers to hydrogen exchange in $\text{H}+\text{H}_2$ ($\sim 5000 \text{ K}$ [16]) and H_2+H_2 ($\sim 60\,000 \text{ K}$ [20]). In the gas phase, conversion by protons and H_3^+ have similar rate coefficients of $\sim 10^{-10} \text{ cm}^3\text{s}^{-1}$ for the $j = 1 \rightarrow 0$ ortho-para transition in the temperature range 10–100 K (see Fig. 7 and [22]). In typical cold molecular clouds, the H_2 density is $\sim 10^4 \text{ cm}^{-3}$ and the relative abundances of H^+ and H_3^+ (relative to H_2) are both a few 10^{-9} . These two ions therefore contribute with similar OPC rates of $\sim 10^{-15} \text{ s}^{-1}$ and the timescale for the gas phase OPC in these objects is $\sim 10 \text{ Myr}$, which is close to the typical lifetime of molecular clouds ($\sim 5 \text{ Myr}$ [87]). As a result, the OPR of H_2 in the cold ISM is expected to be close to its steady-state value, which should however differ from the thermal equilibrium value [10, 13].

In warmer regions such as protostellar shocks or PDRs, the kinetic temperature can exceed 300 K and in this regime collisions with hydrogen atoms become efficient with an OPC rate coefficient larger than $\sim 10^{-16} \text{ cm}^3\text{s}^{-1}$ (see Fig. 4). If the abundance ratio between H and H^+ (or H_3^+) is larger than $\sim 10^6$ (assuming a typical OPC rate coefficient of $\sim 10^{-10} \text{ cm}^3\text{s}^{-1}$ for protons above 100 K), hydrogen atoms will then compete or even dominate the ions in the OPC of H_2 in these environments. At temperatures above $\sim 600 \text{ K}$, the rate coefficient for the conversion of p- H_2 to o- H_2 even exceeds $10^{-13} \text{ cm}^3\text{s}^{-1}$ (Fig. 4). In media where the abundance ratio $[\text{H}] / [\text{H}^+]$ is larger than ~ 1000 , hydrogen atoms will be thus the major para-to-ortho converters with an OPC rate of $\sim 3200 \times (100 \text{ cm}^{-3}/n(\text{H})) \text{ yr}$, where $n(\text{H})$ is the density of hydrogen atoms. Thus, if $n(\text{H})$ is larger than $\sim 10 \text{ cm}^{-3}$, the para-to-ortho conversion by H can yield an equilibrium OPR of 3 within less than 30 000 yr (at kinetic temperatures above 600 K). We note that we do not consider here H_2+H_2 collisions because these have a negligible OPC rate coefficient of $\sim 10^{-27} \text{ cm}^3\text{s}^{-1}$ at 300 K [7]. These collisions can however play a role in the atmospheres of giant (exo)planets owing to H_2 densities much higher than in the ISM.

If we now consider typical dust grains with size $\sim 0.1 \mu\text{m}$, a dust-to-gas ratio of $\sim 10^{-12}$ by number and a H_2 mean velocity of $\sim 3 \times 10^4 \text{ cm.s}^{-1}$, the typical collision rate between H_2 and a dust grain is a few 10^{-14} s^{-1} at 10 K. Using a typical sticking probability of 0.1 [3] and a solid phase OPC efficiency of 1, the overall OPC rate is $\sim 10^{-15} \text{ s}^{-1}$, i.e. similar to the gas phase OPC rate in the cold gas. Dust grains can thus possibly play a role in the OPC of H_2 , in competition with gas phase processes. It should be noted, however, that the OPC efficiency on solid surfaces can be much lower than 1, depending on the ratio between the residence time (which is highly uncertain) and the conversion time (which is typically 10^3 s on amorphous water and graphite) [3, 15]. On the other hand, nascent H_2 molecules formed on a grain could be immediately retrapped in the very irregular surface of amorphous solid water [88]. The OPR of such retrapped H_2 could then reflect the temperature of the surface. In summary, in contrast to the OPC of H_2 by H and H^+ for which rate coefficients are now known with high accuracy, the contribution of dust particles is unclear and more experimental work on interstellar dust analogues is urgently needed. Dedicated astrophysical models including all relevant processes, such as [15], are also necessary to assess the impact of the new calculated rate coefficients.

Finally, in addition to ortho-para conversion, hydrogen atoms and protons are important colliders that can also rotationally excite H_2 molecules, in competition with other H_2 molecules and He atoms (and electrons in highly ionized media). Thus, from data reported in Tables 1-3, we can compare the rate coefficients for ortho-ortho and para-para transitions ($\Delta j = 2$) with those computed for H_2+He and H_2+H_2 [89, 90]. Above 300 K, these latter are similar to those for H_2+H so that all the dominant neutrals (H, He and H_2) significantly contribute to the pure rotational excitation of H_2 . At low temperature ($T \leq 100 \text{ K}$) where data for proton exchange are available, the rate coefficients for the transitions $j = 0 \rightarrow 2$ and $j = 1 \rightarrow 3$ are 3-4 orders of magnitude larger for protons than for neutrals. The contribution of protons in the rotational excitation of H_2 ($\Delta j = 2$) is therefore significant if their relative abundance (with respect to the dominant neutral) exceeds $\sim 10^{-4}$, e.g. in the early universe [2].

V. CONCLUSION

We have attempted to review the recent achievements related to the gas phase ortho–para conversion of H_2 in astrophysical media. Despite these new data already improve significantly the modeling of this process in interstellar media and early universe, there is still a lack of data for high temperatures and for high ro-vibrational levels, including for pure ro-vibrational excitation. Extrapolation to higher (lower) temperatures is addressed for example in Ref. [91] where specific analytic extrapolation formulae are suggested. The danger of extrapolation is however emphasized by Flower and Pineau des Forêts [92] for a number of molecules including H_2 and we endorse these warnings on an even larger scale.

Thus, it seems important to extend the present calculations in order to provide the astronomers the necessary tools to model the ro-vibrational excitation and ortho–para- H_2 conversion processes in hot environments. Such extension should be feasible for the ortho–para- H_2 conversion by hydrogen exchange since the calculations are relatively fast in terms of CPU time. At the opposite, for ortho–para- H_2 conversion by proton exchange, an extension to higher temperature may be more difficult since it will imply to deal with a huge number of coupled channels using the quantum time independent approach. Statistical method may be then an interesting alternative since quantum and statistical approach are generally in good agreement for this system.

Acknowledgments

FL, PH and AF acknowledge the CNRS national program “Physique et Chimie du Milieu Interstellaire”. F.L. is grateful for the financial support of the CPER Haute-Normandie/CNRT/Energie, Electronique, Matériaux. F.L. and A.F. acknowledge support by the Agence Nationale de la Recherche (ANR-HYDRIDES), contract ANR-12-BS05-0011-01.

-
- [1] N. Watanabe and A. Kouchi, *Progress In Surface Science* **83**, 439 (2008).
 - [2] D. Galli and F. Palla, *Ann. Rev. Astron. Astrophys.* **51**, 163 (2013), 1211.3319.
 - [3] K. Fukutani and T. Sugimoto, *Progress In Surface Science* **88**, 279 (2013).

- [4] L. Pagani, C. Vastel, E. Hugo, V. Kokoouline, C. H. Greene, A. Bacmann, E. Bayet, C. Ceccarelli, R. Peng, and S. Schlemmer, *A&A* **494**, 623 (2009), 0810.1861.
- [5] K. Pachucki and J. Komasa, *Phys. Rev. A* **77**, 030501 (2008).
- [6] T. Sugimoto and K. Fukutani, *Nature Physics* **7**, 307 (2011).
- [7] D. L. Huestis, *Planetary Space Science* **56**, 1733 (2008).
- [8] D. A. Neufeld, G. J. Melnick, and M. Harwit, *ApJL* **506**, L75 (1998).
- [9] S. Maret, E. A. Bergin, D. A. Neufeld, J. D. Green, D. M. Watson, M. O. Harwit, L. E. Kristensen, G. J. Melnick, P. Sonnentrucker, V. Tolls, et al., *Astrophys. J.* **698**, 1244 (2009), 0904.0603.
- [10] D. R. Flower, G. Pineau Des Forêts, and C. M. Walmsley, *A&A* **449**, 621 (2006).
- [11] L. Pagani, P. Lesaffre, M. Jorfi, P. Honvault, T. González-Lezana, and A. Faure, *A&A* **551**, A38 (2013).
- [12] V. Dislaire, P. Hily-Blant, A. Faure, S. Maret, A. Bacmann, and G. Pineau Des Forêts, *A&A* **537**, A20 (2012), 1111.1572.
- [13] A. Faure, P. Hily-Blant, R. Le Gal, C. Rist, and G. Pineau des Forêts, *ApJL* **770**, L2 (2013).
- [14] N. Troscompt, A. Faure, S. Maret, C. Ceccarelli, P. Hily-Blant, and L. Wiesenfeld, *Astron. Astrophys.* **506**, 1243 (2009).
- [15] J. Le Bourlot, *A&A* **360**, 656 (2000).
- [16] F. Lique, P. Honvault, and A. Faure, *J. Chem. Phys.* **137**, 154303 (2012).
- [17] P. Honvault, M. Jorfi, T. González-Lezana, A. Faure, and L. Pagani, *Phys. Rev. Lett.* **107**, 023201 (2011).
- [18] P. Honvault, M. Jorfi, T. González-Lezana, A. Faure, and L. Pagani, *Physical Chemistry Chemical Physics (Incorporating Faraday Transactions)* **13**, 19089 (2011).
- [19] P. Honvault, M. Jorfi, T. González-Lezana, A. Faure, and L. Pagani, *Phys. Rev. Lett.* **108**, 109903 (2012).
- [20] E. Carmona-Novillo, M. Bartolomei, M. I. Hernández, and J. Campos-Martínez, *J. Chem. Phys.* **126**, 124315 (2007).
- [21] F. Grussie, M. H. Berg, K. N. Crabtree, S. Gärtner, B. J. McCall, S. Schlemmer, A. Wolf, and H. Kreckel, *Astrophys. J.* **759**, 21 (2012), 1209.3041.
- [22] S. Gómez-Carrasco, L. González-Sánchez, A. Aguado, C. Sanz-Sanz, A. Zanchet, and O. Roncero, *J. Chem. Phys.* **137**, 094303 (2012).

- [23] H.-J. Werner, P. J. Knowles, G. Knizia, F. R. Manby, and M. Schütz, *Wiley Interdisciplinary Reviews: Computational Molecular Science* **2**, 242 (2012), ISSN 1759-0884, URL <http://dx.doi.org/10.1002/wcms.82>.
- [24] H.-J. Werner and P. J. Knowles, *J. Chem. Phys.* **89**, 5803 (1988).
- [25] P. Knowles, *Chem. Phys. Lett.* **145**, 514 (1988).
- [26] P. J. Knowles and N. C. Handy, *Chem. Phys. Lett.* **111**, 315 (1984).
- [27] P. J. Knowles and N. C. Handy, *Comp. Phys. Commun.* **54**, 75 (1989).
- [28] K. Andersson, P.-Å. Malmqvist, and B. O. Roos, *J. Chem. Phys.* **96**, 1218 (1992).
- [29] P. Celani and H.-J. Werner, *J. Chem. Phys.* **112**, 5546 (2000).
- [30] I. Shavitt and R. Bartlett, *Many-Body Methods in Chemistry and Physics: MBPT and Coupled-Cluster Theory*, Cambridge Molecular Science (Cambridge University Press, 2009), ISBN 9780521818322, URL <http://books.google.co.uk/books?id=SWw6ac1NHZYC>.
- [31] R. A. Kendall, T. H. Dunning, and R. J. Harrison, *J. Chem. Phys.* **96**, 6796 (1992).
- [32] D. E. Woon and T. H. Dunning, Jr., *J. Chem. Phys.* **98**, 1358 (1993).
- [33] D. E. Woon and T. H. Dunning, *J. Chem. Phys.* **100**, 2975 (1994).
- [34] K. A. Peterson, D. E. Woon, and T. H. Dunning, Jr., *J. Chem. Phys.* **100**, 7410 (1994).
- [35] D. Feller and J. A. Sordo, *J. Chem. Phys.* **112**, 5604 (2000).
- [36] MOLPRO is a package of *ab initio* programs written by H.-J. Werner and P. J. Knowles, with contributions from R. D. Amos, A. Berning, D. L. Cooper, M. J. O. Deegan, A. J. Dobbyn, F. Eckert, C. Hampel, T. Leininger, R. Lindh, A. W. Lloyd, W. Meyer, M. E. Mura, A. Nicklaß, P. Palmieri, K. Peterson, R. Pitzer, P. Pulay, G. Rauhut, M. Schütz, H. Stoll, A. J. Stone and T. Thorsteinsson.
- [37] M. J. Frisch, G. W. Trucks, H. B. Schlegel, G. E. Scuseria, M. A. Robb, J. R. Cheeseman, G. Scalmani, V. Barone, B. Mennucci, G. A. Petersson, et al., *Gaussian 09 Revision A.1*, gaussian Inc. Wallingford CT 2009.
- [38] F. Aquilante, L. De Vico, N. Ferré, G. Ghigo, P.-r. Malmqvist, P. Neogrády, T. B. Pedersen, M. Pitoňák, M. Reiher, B. O. Roos, et al., *J. Comput. Chem.* **31**, 224 (2010), URL <http://dx.doi.org/10.1002/jcc.21318>.
- [39] T.-S. Ho and H. Rabitz, *J. Chem. Phys.* **104**, 2584 (1996).
- [40] A. J. C. Varandas, *Intermolecular and Intramolecular Potentials: Topographical Aspects, Calculation, and Functional Representation via A Double Many-Body Expansion*

- Method* (John Wiley & Sons, Inc., 2007), pp. 255–338, ISBN 9780470141236, URL <http://dx.doi.org/10.1002/9780470141236.ch2>.
- [41] A. J. Stone, *The Theory of Intermolecular forces* (Clarendon Press, Oxford, 1996).
- [42] D. G. Truhlar and C. J. Horowitz, *J. Chem. Phys.* **68**, 2466 (1978).
- [43] P. Siegbahn and B. Liu, *J. Chem. Phys.* **68**, 2457 (1978).
- [44] A. J. C. Varandas, F. B. Brown, C. A. Mead, D. G. Truhlar, and N. C. Blais, *J. Chem. Phys.* **86**, 6258 (1987).
- [45] A. I. Boothroyd, P. G. Martin, W. J. Keogh, and M. R. Peterson, *J. Chem. Phys.* **95**, 4343 (1991).
- [46] A. I. Boothroyd, W. J. Keogh, P. G. Martin, and M. R. Peterson, *J. Chem. Phys.* **104**, 7139 (1996).
- [47] S. L. Mielke, B. C. Garrett, and K. A. Peterson, *J. Chem. Phys.* **116**, 4142 (2002).
- [48] A. Aguado, O. Roncero, C. Tablero, C. Sanz, and M. Paniagua, *J. Chem. Phys.* **112**, 1240 (2000).
- [49] T. Takayanagi, Y. Kurosaki, and A. Ichihara, *J. Chem. Phys.* **112**, 2615 (2000).
- [50] H. Kamisaka, W. Bian, K. Nobusada, and H. Nakamura, *J. Chem. Phys.* **116**, 654 (2002).
- [51] L. P. Viegas, A. Alijah, and A. J. C. Varandas, *J. Chem. Phys.* **126**, 074309 (2007).
- [52] L. Velilla, B. Lepetit, A. Aguado, J. A. Beswick, and M. Paniagua, *J. Chem. Phys.* **129**, 084307 (2008).
- [53] P. Honvault and Y. Scribano, *Journal of Physical Chemistry A* **117**, 9778 (2013).
- [54] P. Honvault and Y. Scribano, *The Journal of Physical Chemistry A* **117**, 13205 (2013), <http://pubs.acs.org/doi/pdf/10.1021/jp4113377>, URL <http://pubs.acs.org/doi/abs/10.1021/jp4113377>.
- [55] A. M. Arthurs and A. Dalgarno, *Proc. R. Soc. A* **256**, 540 (1960).
- [56] G. C. Schatz and A. Kuppermann, *J. Chem. Phys.* **65**, 4642 (1976).
- [57] A. Kuppermann, J. A. Kaye, and J. P. Dwyer, *Chemical Physics Letters* **74**, 257 (1980).
- [58] D. Skouteris, J. Castillo, and D. Manolopoulos, *Comput. Phys. Commun.* **133**, 128 (2000).
- [59] P. Honvault and J.-M. Launay, in *Chemical Reaction Dynamics*, edited by A. Laganá and G. Lendvay (Kluwer Academic, Amsterdam, NL, 2004), p. 187.
- [60] Y.-S. Mark Wu, A. Kuppermann, and B. Lepetit, *Chemical Physics Letters* **186**, 319 (1991).
- [61] W. H. Miller, *J. Chem. Phys.* **50**, 407 (1969).

- [62] D. G. Truhlar, J. Chem. Phys. **65**, 1008 (1976).
- [63] T. González-Lezana, P. Honvault, and Y. Scribano, J. Chem. Phys. **139**, 054301 (2013).
- [64] L. Bonnet and J. Rayez, Chem. Phys. Lett. **397**, 106 (2004).
- [65] M. E. Mandy, Chem. Phys. **365**, 1 (2009).
- [66] E. J. Rackham, F. Huarte-Larranaga, and D. E. Manolopoulos, Chemical Physics Letters **343**, 356 (2001).
- [67] E. J. Rackham, T. Gonzalez-Lezana, and D. E. Manolopoulos, J. Chem. Phys. **119**, 12895 (2003).
- [68] D. R. Flower, MNRAS **288**, 627 (1997).
- [69] S. A. Wrathmall and D. R. Flower, J. Phys. B **39**, L249 (2006).
- [70] M. E. Mandy and P. G. Martin, J. Chem. Phys. **97**, 265 (1992).
- [71] Y. Sun and A. Dalgarno, Astrophys. J. **427**, 1053 (1994).
- [72] W. R. Schulz and D. J. Le Roy, J. Chem. Phys. **42**, 3869 (1965).
- [73] F. Bouakline, B. Lepetit, S. C. Althorpe, and A. Kuppermann, in *Springer Series in Chemical Physics 97*, edited by D. R. Y. H Koppel and H. Barentzen (Springer, New York, 2010).
- [74] C. A. Mead and D. G. Truhlar, J. Chem. Phys. **70**, 2284 (1979).
- [75] B. Lepetit and A. Kupperman, Chem. Phys. Lett. **166**, 581 (1980).
- [76] F. J. Aoiz, L. Bañares, and V. J. Herrero, Int. Rev. in Phys. Chem. **24**, 119 (2005).
- [77] L. Che, Z. Ren, X. Wang, W. Dong, D. Dai, X. Wang, D. H. Zhang, X. Yang, G. Li, H.-J. Werner, et al., Science **317**, 1061 (2007).
- [78] F. Lique, G. Li, H.-J. Werner, and M. H. Alexander, J. Chem. Phys. **134**, 231101 (2011).
- [79] X. Wang, W. Dong, C. Xiao, L. Che, Z. Ren, D. Dai, X. Wang, P. Casavecchia, X. Yang, B. Jiang, et al., Science **322**, 573 (2008).
- [80] S. L. Mielke, K. A. Peterson, D. W. Schwenke, B. C. Garrett, D. G. Truhlar, J. V. Michael, M.-C. Su, and J. W. Sutherland, Phys. Rev. Lett. **91**, 063201 (2003).
- [81] J. M. Hutson and S. Green, MOLSCAT computer code, version 14 (1994), distributed by Collaborative Computational Project No. 6 of the Engineering and Physical Sciences Research Council (UK).
- [82] F. Lique and A. Faure, J. Chem. Phys. **136**, 031101 (2012).
- [83] D. Gerlich, J. Chem. Phys. **92**, 2377 (1990).
- [84] T. González-Lezana, O. Roncero, P. Honvault, J.-M. Launay, N. Bulut, F. Javier Aoiz, and

- L. Bañares, *J. Chem. Phys.* **125**, 094314 (2006).
- [85] F. J. Aoiz, V. Sáez Rábanos, T. González-Lezana, and D. E. Manolopoulos, *J. Chem. Phys.* **126**, 161101 (2007).
- [86] D. Gerlich, R. Plasil, I. Zymak, M. Hejduk, P. Jusko, D. Mulin, and J. Glosik, *J. Phys. Chem. A* **117**, 10068 (2013).
- [87] E. A. Bergin and M. Tafalla, *Ann. Rev. Astron. Astrophys.* **45**, 339 (2007), 0705.3765.
- [88] N. Watanabe, Y. Kimura, A. Kouchi, T. Chigai, T. Hama, and V. Pirronello, *ApJL* **714**, L233 (2010).
- [89] N. Balakrishnan, R. C. Forrey, and A. Dalgarno, *Astrophys. J.* **514**, 520 (1999).
- [90] T.-G. Lee, N. Balakrishnan, R. C. Forrey, P. C. Stancil, G. Shaw, D. R. Schultz, and G. J. Ferland, *Astrophys. J.* **689**, 1105 (2008), 0805.1623.
- [91] F. L. Schöier, F. F. S. van der Tak, E. F. van Dishoeck, and J. H. Black, *A&A* **432**, 369 (2005).
- [92] D. R. Flower and G. Pineau des Forêts, *MNRAS* **421**, 2786 (2012).